Assessment of turbulence model predictions for a centrifugal compressor simulation

Proceedings of the 1st Global Power and Propulsion Forum
GPPF 2017
Jan 16-18, 2017, Zurich, Switzerland
www.pps.global

GPPF-2017-0138

ASSESSMENT OF TURBULENCE MODEL PREDICTIONS FOR A CENTRIFUGAL COMPRESSOR SIMULATION

Lee Gibson, Lee Galloway, Sung in Kim*, Stephen Spence
Queen's University Belfast
Belfast, United Kingdom
**Corresponding author: s.kim@qub.ac.uk*

ABSTRACT

Steady-state computational fluid dynamics (CFD) simulations are an essential tool in the design process of centrifugal compressors. Whilst global parameters, such as pressure ratio and efficiency, can be predicted with reasonable accuracy, the accurate prediction of detailed compressor flow fields is a much more significant challenge. Much of the inaccuracy is associated with the incorrect selection of turbulence model. The need for a quick turnaround in simulations during the design optimisation process, also demands that the turbulence model selected be robust and numerically stable with short simulation times.

In order to assess the accuracy of a number of turbulence model predictions, the current study used an exemplar open CFD test case, the centrifugal compressor '*Radiver*', to compare the results of three eddy viscosity models and two Reynolds stress type models. The turbulence models investigated in this study were (i) Spalart-Allmaras (SA) model, (ii) the Shear Stress Transport (SST) model, (iii) a modification to the SST model denoted the SST-curvature correction (SST-CC), (iv) Reynolds stress model of Speziale, Sarkar and Gatski (RSM-SSG), and (v) the turbulence frequency formulated Reynolds stress model (RSM-ω). Each was found to be in good agreement with the experiments (below 2% discrepancy), with respect to total-to-total parameters at three different operating conditions. However, for the off-design conditions, local flow field differences were observed between the models, with the SA model showing particularly poor prediction of local flow structures. The SST-CC showed better prediction of curved rotating flows in the impeller. The RSM-ω was better for the wake and separated flow in the diffuser. The SST model showed reasonably stable, robust and time efficient capability to predict global and local flow features.

1 INTRODUCTION

The design of centrifugal compressors requires the use of computational methods in conjunction with experimental validation to provide accurate analysis with a quick turn-around between design iterations. The difficulty that arises when using computational methods is the simulation turnover time, which depends heavily on the grid used, boundary conditions applied and the turbulence model employed. Full stage unsteady simulations are currently too costly and time consuming for the iterative design process. Steady-state models which use a mixing plane method to model the interface between rotating and stationary domains are preferred due to the considerably reduced simulation time. However, the importance of turbulence model chosen still plays a significant role in achieving realistic predictions of the compressor performance.

Turbulence modelling attempts to model turbulent flow behaviour using a set of partial differential equations based on appropriate approximations of the exact Navier-Stokes equations [1]. There are two types of Reynolds Averaged Navier Stokes (RANS) models that either i) use the turbulent (or eddy) viscosity μ_t to calculate the Reynolds stresses or ii) solve an equation for each of the Reynolds stresses. The eddy viscosity models use the Boussinesq approximation, defined as the product of the eddy viscosity and mean strain rate tensor to calculate the Reynolds stresses (Eq. 1).

$$-\rho\overline{u_i' u_j'} = \mu_t\left(\frac{\partial u_i}{\partial x_j}+\frac{\partial u_j}{\partial x_i}\right)-\frac{2}{3}\left(\rho k+\mu_t\frac{\partial u_k}{\partial x_k}\right)\delta_{ij} \qquad (1)$$

The eddy viscosity is calculated as a function of the modelled turbulent variables. This method assumes that the Reynolds stresses are isotropic, which is a valid assumption for simple flows. However, the Reynolds stresses are found to be anisotropic in complex swirling flows such as those present within a centrifugal compressor [1]. Theoretically, the downside of eddy viscosity models is that they are unable to properly account for streamline curvature, body forces and history effects on the individual components of the Reynolds stress tensor [2]. Therefore, Reynolds stress models have potential advantages over their eddy-viscosity counterparts. However, with respect to centrifugal compressor flows, this is often not the case and strong similarities often exist between the two with respect to local flow field structure and

performance parameter predictions. There are many different formulations of turbulence model, both of the eddy viscosity and Reynolds stress type. The main factors that influences the selection process are the computational cost, grid requirements, ability to capture realistic flow physics, and accuracy.

2 SCOPE OF PAPER

The present work is a comparative study of several different turbulence models used in the steady state simulation of a centrifugal compressor stage with a vaned diffuser. The performance and flow field predictions are evaluated against available experimental data and the results of each turbulence model are discussed. The primary objective of the present study is to propose a stable, numerically robust and accurate turbulence model suitable for application to flows within a centrifugal compressor over a broad range of operating conditions.

3 CENTRIFUGAL COMPRESSOR STAGE

The centrifugal compressor stage used for the assessment of turbulence model predictions was the exemplar open CFD test case, entitled '*Radiver*' [3, 4]. The compressor stage consists of an unshrouded impeller with 15 backswept blades and 23-vane wedge type diffuser. Numerical simulations were carried at 80% design speed due to the increased amount of experiment data available at this speed. Details of the impeller and diffuser geometry are shown in Table 1.

Table 1 Compressor details for 4% radial gap at 80% speed

Shaft speed (80%)	28,541 rpm
Tip radius	135 mm
Number of impeller blades	15
Blade backsweep angle at impeller exit	38°
Impeller leading edge tip clearance	0.70 mm
Impeller trailing edge tip clearance	0.48 mm
Number of diffuser vanes	23
Diffuser vane angle	16.50°
Diffuser channel height	11.10 mm
Diffuser leading edge radius	140.40 mm
Plane 2M radius	138.10 mm
Plane 8M radius	335 mm

4 NUMERICAL DETAILS

4.1 Solver

Simulations were carried out using the commercial CFD code ANSYS CFX 16.2. A high resolution advection scheme was used to solve the discretised conservation equations and mass flow was evaluated using the high resolution velocity-pressure algorithm of Rhie and Chow based on the numerical set-up of Bourgeois et al. [5]. Second order turbulence numerics and a turbulence intensity of 5% were assumed at the inlet of the computational domain according to recommendations [6] and a similar case [7]. Conservation of energy was evaluated using the total energy equation with the viscous work term included to capture any heat generation due to viscosity.

4.2 Modelling approach

Numerical simulations were performed using a steady-state, single passage model with periodic boundary conditions, as shown in Fig. 1. Structured hexahedral grids for the compressor passages were generated using the dedicated ANSYS meshing tool TurboGrid.

A stage interface was used at the interface of the rotating impeller and stationary diffuser domains. The stage interface performs a circumferential averaging of the fluxes at the exit plane of the rotating domain to construct spanwise profiles of the conserved variables at the inlet of the stationary domain. Stage averaging between the blade passages accounts for time averaging effects, thus the results therefore do not depend on the relative position between the two components.

Since the collector at the outlet of the diffuser is not included in this analysis, the computational domain is restricted between an inlet plane 50 mm upstream of the impeller leading edge (the measurement plane 1) to shortly downstream of the diffuser exit (8M, according to the notation in [3, 4]). Thus, the performance is calculated between the planes 1-8M. This is also similar to the computational setup used by Smirnov et al. [7].

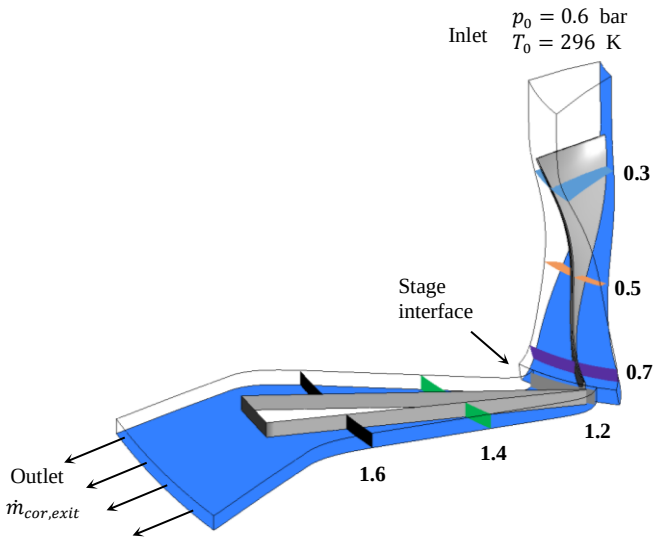

Fig. 1 Computational domain and boundary conditions

4.3 Boundary conditions

The inlet conditions were specified as a total pressure of 0.6 bar and a total temperature of 296 K (23℃) based on recommendations by the authors of the test case. The fluid is defined as Air Ideal Gas and the no-slip boundary condition was used at all solid wall surfaces. The specific heat capacity at constant pressure C_p and ratio of specific heats γ are 1005 J/kg·K and 1.4, respectively.

It is known that CFD solvers run into difficulty at/near the surge and choke conditions depending on the boundary

condition specified. Typically, a static pressure boundary condition is placed at the outlet near choke conditions and a mass flow rate boundary condition near surge [5, 8]. In this analysis, the exit corrected mass flow rate, $m_{cor,exit}$ has been used. It is a function of the mass flow rate, and mass averaged total temperature and pressure at the outlet plane [6]. This makes it more stable compared to a static pressure or regular mass flow rate condition. Finally, the location of the impeller-diffuser interface is mid-way between the radial gap of 4%. This corresponds to a radius of 137.7 mm from the axis of rotation of the impeller.

Three operating points were simulated along the 80% speedline (P1 [near surge], M [mid-map] and S1 [near choke]) to achieve a broad view of how the turbulence models perform at different operating conditions.

4.4 Grid convergence study

A grid convergence analysis was carried out to ensure that the solution is independent from the grid and the discretisation error is low. Three grids (coarse, medium and fine) were simulated at the operating points P1, M and S1 using the SST turbulence model. This model was chosen for its numerical stability over a range of operating conditions [5]. Also, the converged mesh can be applied to the SST-CC and RSM-ω models due to their similar grid requirements. A target y^+ value of 0.7 was used to ensure the change in turbulence model did not have a profound effect and to have a good boundary layer resolution. The number of elements for each grid from coarse to fine was 0.5 million (0.5M), 1M and 2M. The used convergence criteria were that RMS residuals reach less than 1E-04, and the global imbalances of mass, momentum and energy are less than 0.1%. The percentage change in several overall parameters for operating point P1 are shown in Table 2. It is clear that the discrepancy for the first grid refinement (coarse to medium) is much more significant than the second refinement (medium to fine).

Table 2 Absolute percentage discrepancy between grid refinements

	$\eta_{01,08M}$	$\Pi_{01,08M}$	$\eta_{01,8M}$	$\Pi_{01,8M}$	$TR_{01,08M}$
C-M	1.46	1.07	3.18	2.48	0.05
M-F	0.41	0.50	0.57	0.63	0.04

Another method used for analysing the simulations for grid independence was by comparing circumferentially mass averaged, spanwise velocity profiles at a number of locations through the compressor stage. The streamwise locations of the turbosurfaces used to compute the velocity profiles can be seen in Fig. 1. The velocity profiles are non-dimensionalised by the blade tip speed U_2 (≈ 403 m/s). In the rotating and stationary frames of reference, the relative and absolute velocities are used respectively.

The normalised velocity is shown in Fig. 2 for operating point P1, where the line colours correspond to the streamwise planes defined in Fig. 1. The coarse grid shows a larger difference in diffuser downstream compared to the medium and fine grids. This is due to an increased level of blockage predicted within the diffuser channel compared to the other two grids, where specifically, the coarse grid predicts 25% and the medium and fine grids predict approximately 15% channel blockage. Based on the results of the grid convergence analysis, the medium grid is chosen as a trade-off between accuracy and computational solving time.

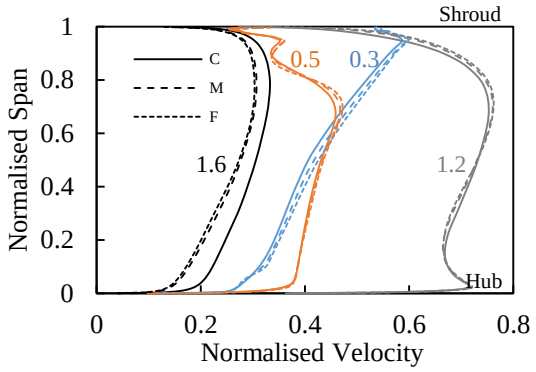

Fig. 2 Velocity profiles of different grids at various streamwise locations at the operating point, P1

5 SELECTED TURBULENCE MODELS

5.1 Eddy-viscosity models

The first eddy-viscosity model considered in this study is the Shear Stress Transport (SST) model which is a combination of the k-ϵ and k-ω in which the former model is used for free stream flow and the latter is used for modelling near the wall. Mathematical blending functions are employed to switch between models without user interaction [9]. The SST has been applied frequently to centrifugal compressors in recent times as it provides good predictions of the flow field and compressor performance over a broad range of operating conditions. However, it is not perfect as it often over predicts the total pressure rise [10].

Since eddy viscosity models are insensitive to streamline curvature and system rotation, a number of modifications have been suggested to sensitise them with little solver implementation and effort. Spalart and Shur [11] proposed a modification to the production term P_k in order to sensitise eddy viscosity models to these effects, called SST curvature correction function (SST-CC). In regions of enhanced turbulence production such as a strong concave surface, the multiplication factor takes on a maximum value of 1.25 whereas in regions of no turbulence production such as a strong convex surface, a value of 0 is used.

The other eddy-viscosity model investigated is the Spalart-Allmaras (SA) turbulence model. This one-equation turbulence model uses a transport equation for the modified turbulent kinematic viscosity [2]. The major advantage of this model is that it uses only one transport equation, as opposed to two of the SST model, making it efficient with respect to computational time.

5.2 Reynolds stress models

The RSM-SSG turbulence model solves for each Reynolds stress using the turbulence dissipation rate ϵ, a quadratic pressure-strain correlation and employs scalable wall functions [4]. Johnson [12] states that the pressure-strain correlation "represents the redistribution of energy between different components of the turbulence" and that the additional terms proposed by Speziale, Sarkar and Gatski (SSG) provide a more accurate representation of turbulent flows.

The RSM-ω model solves for each of the Reynolds stresses using the turbulence frequency ω as the transport variable. An advantage of this model over the RSM-SSG is that it does not use the turbulence dissipation rate ϵ which is found to be problematic in regions of large separation. Furthermore, automatic wall functions are employed to provide accurate resolution into the boundary layer based on the grid used. Whilst the current literature does not show much application to turbomachinery flows, Fletcher et al. [13] found that the results obtained were similar to the SST when investigating turbulent flow and heat transfer in a square-section duct.

6 RESULTS AND DISCUSSION

The following sections present the results obtained by each turbulence model. Where possible, predictions are compared to experimental data. One-dimensional data is available for all operating points considered e.g. pressure and temperature whereas local experimental contour plots are available only for the operating points P1 and M.

6.1 Global speedlines

Firstly, the global performance predictions of the compressor stage are presented in the form of speedlines. Speedlines are shown in Fig. 3 for a number of different performance measures of the compressor. The reference point used to normalise data is the experimental data at the operating point M. Each model predicts the performance of the compressor in good agreement with the experiment in most cases, where the differences from the experiment are generally quite small (less than 2% in most cases). The pressure ratio is predicted in good agreement with the experiment by each turbulence model. However, the total-to-total efficiency suffers because of the discrepancy in total temperature at the outlet, particularly near the choke condition. The absolute percentage discrepancy between experimental and numerical results for the operating point P1 is listed in Table 3.

SA predicts the total-to-total pressure and temperature ratio in good agreement with the experiment at the operating point P1 and it predicts the total-to-total efficiency most accurately of all the models considered. However, it is the least accurate in terms of total-to-static efficiency. The reason for this is addressed in detail later. The curvature correction applied to the SST model has been found to reduce the discrepancy in terms of total-to-total pressure ratio. This is in agreement with Smirnov et al. [10] and Ali et al. [14]. However, the main drawback of the correction is in the form of a slightly reduced work input (due to the lower total temperature at the outlet relative to the original SST model, see Fig. 3 (b)) which has not been reported by the aforementioned authors. The RSM-SSG is slightly better than the ω formulated model (RSM-ω). However, the differences between the models are not significant.

Table 3 Absolute percentage discrepancy between experimental and numerical results for P1

	SST	SST-CC	SA	RSM-SSG	RSM-ω
$\Pi_{01,08M}$	0.69	0.28	0.64	0.68	0.77
$\eta_{01,08M}$	1.83	1.61	0.77	1.77	2.18
$\eta_{01,8M}$	0.83	1.05	3.43	1.48	1.33
$TR_{01,08M}$	0.27	0.35	0.01	0.27	0.35

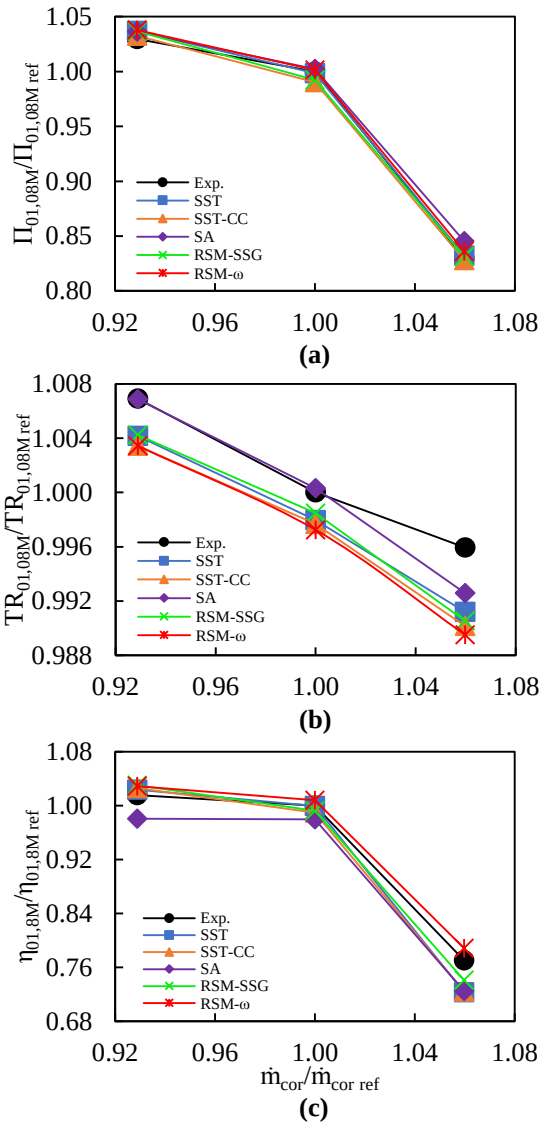

Fig. 3 Global performance parameters (a) total-to-total pressure ratio, (b) total-to-total temperature ratio, and (c) total-to-static efficiency

The operating point M is predicted with better accuracy than P1, where differences are well below 1% in most cases. An interesting feature at this operating point is the shifting of the RSM-SSG and SST-CC below the experiment with respect to total-to-static efficiency (Fig. 3 (c)). Inspection of the static pressure at diffuser exit highlights that both models under predict the static pressure by 1.04% (RSM-SSG) and 1.50% (SST-CC and SA). This, in combination with a reduced work input predicted, is the main contributor towards a lower efficiency prediction.

Near the choke condition (S1), the performance is not relatively well predicted by many of the models. The reason is attributed to the flow becoming highly separated within the diffuser. An interesting feature at this point is that the RSM-ω is the only one to over predict the total-to-static efficiency whereas the other models are found to under predict this parameter. This is attributed to the small discrepancy in static pressure at diffuser outlet: 0.15% where the others predicted well above 3%. Conclusively, all five models provide the overall performance parameters within an acceptable range of accuracy for the present test cases.

6.2 LOCAL MEASUREMENT PLANE COMPARISON

6.2.1 Impeller exit: Measurement plane 2M'

For the off-design operating condition, P1, absolute (c), meridional (c_r), circumferential (c_θ), and relative (w) velocity distributions were compared at the impeller exit plane, 2M'. The circumferential velocity contours among those are shown in Fig. 4. In general, the curvature correction form of the SST model (SST-CC) showed the best prediction of the local flow structures of curved rotating flows in the impeller, whilst SA showed the least accurate flow field prediction. There were close similarities between the SST-CC and RSM-SSG models although the RSM-SSG magnified the intensity of localised features near the shroud. With regard to the SA, it is unique in that it did not predict highly localised zones like the others i.e. the flow field was more homogenous indicating less mixing loss.

6.2.2 Diffuser exit: Measurement plane 7M

The experiments by Ziegler et al. [3, 4] found that the size of the radial gap influenced which side the maximum total pressure was biased towards in the diffuser channel at a fixed operating point. For example, at the operating point P1 for the 14% gap it was biased towards the suction side and moved towards the pressure side with decreasing radial gap. For the 4% gap, the total pressure was expected to be biased towards the pressure side and centre of the channel respectively for P1 and M respectively. Inspection of each turbulence model highlighted that the best model to predict the similar flow structure at this plane for the operating point P1 was RSM-ω, although the wake was predicted larger near the pressure side (Fig. 5). In this off design condition, the separated flow and wake are the key flow features and discussed further in the succeeding section. The most unphysical model was the SA which showed a very highly loaded suction side compared to others which are more central. Although most models predicted the overall performance parameters in good agreement with the experiment, this doesn't imply that the flow features are too. In cases where the local flow structures must be accurately captured, SA does not appear to be an appropriate model.

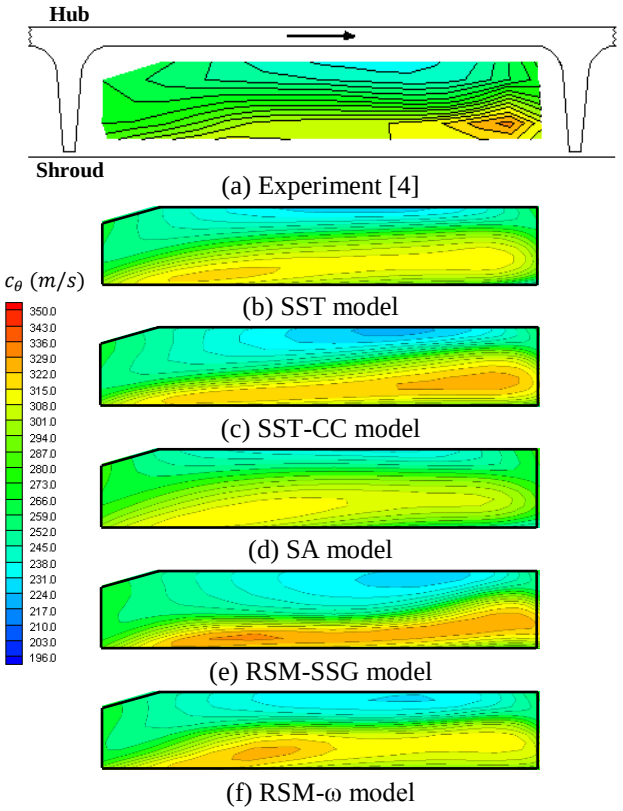

Fig. 4 Circumferential velocity contours for different turbulence models at the impeller exit (the plane 2M') and the operating point, P1

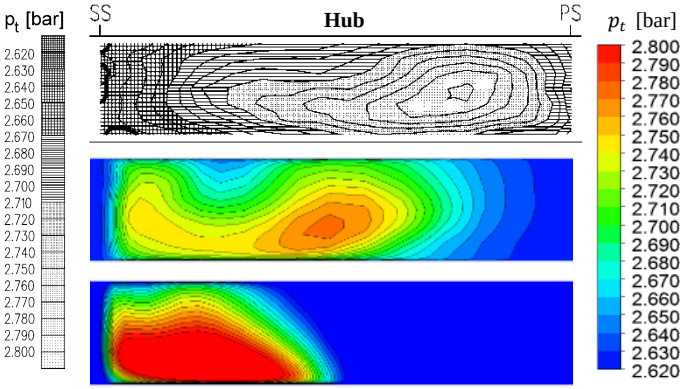

Fig. 5 Contour plots of total corrected pressure at the measurement plane 7M (at the operating point, P1): experiment (top), RSM-ω (middle), SA (bottom)

6.3 BLOCKAGE AND LOSS

Blockage has an adverse effect on the flow due to thick boundary layers altering the geometry of the flow passage.

Unfortunately, there is no experimental data available to calculate the level of blockage at 2M'. However, it is interesting to inspect how blockage predictions at the impeller trailing edge varies between models at the operating point P1. In addition, the static pressure rise c_p and stagnation pressure loss Y_p coefficient through the diffuser are presented in Table 4, for which there are experimental data available for comparison. Both coefficients are evaluated between planes 2M and 7M i.e. just upstream of the diffuser leading edge and just downstream of the diffuser channel exit.

Most models predict the static pressure rise across the diffuser in good agreement with the experiment, particularly the SST and RSM-ω, whereas the stagnation pressure loss is slightly lower for all models but the SA. The values of c_p and Y_p reported by the SA model are not surprising since it has predicted the lowest total-to-static efficiency. The reasons for this are detailed below.

Table 4 Comparison of various parameters at P1

	SST	SST-CC	SA	RSM-SSG	RSM-ω	Exp
c_p	0.75	0.76	0.62	0.77	0.76	0.75
Y_p	0.14	0.14	0.19	0.15	0.14	0.17
B_2 (%)	16.32	17.66	14.84	14.34	13.58	-

The diffuser vane wake produces a large level of loss within the diffuser domain due to recirculating flow that mixes with the flow exiting the diffuser channel near the suction side and also re-enters the separated pressure side flow. Figure 6 highlights this for the SA model which is found to predict the largest level of separation and lowest static pressure rise at the operating point P1. A closer inspection using three-dimensional velocity streamlines suggests that a clockwise rotating vortex (as viewed from above) and the pressure difference between the outlet and further upstream is the mechanism behind the wake flow mixing with the separated flow on the pressure side of the vane. Although back flow downstream of the diffuser near the collector (which was not modelled) has been reported in the experimental test case, the magnitude of this has not been quantified. Therefore, in the case of the SA model, the location of the outlet plane at 8M may magnify the effect of the vortex behind the diffuser vane compared to the other models.

Since the SST model predicts the static pressure rise and the stagnation pressure loss coefficient in good agreement with the experiment, this model was used as a basis for comparison to the SA model with respect to entropy within the diffuser channel (Fig. 7). Furthermore, at this off-design operating point (P1), the SST predicts the static pressure and total-to-static efficiency best out of all models (-0.03% and 0.833% respectively) implying that this model reflects the experiment realistically with respect to one-dimensional values.

Within the diffuser channel, the SA model predicts a high level of entropy generation beginning shortly downstream of the diffuser throat, which spreads towards the centre of the channel, mixing with the low entropy flow near the suction side, and subsequently introduces further losses. On the other hand, the SST model predicts a similar level of entropy generation downstream of the diffuser throat on the pressure side in a relatively small region, but does not tend to spread further downstream. This relatively short passage of high entropy generation of the SST model is due to a small separation bubble near the shroud, whereas the SA model shows larger flow separation. Figure 8 shows a static pressure plot at 95% span in the diffuser domain with streamlines superimposed. The location of the separation bubble at the pressure side of the diffuser channel is visible and it can also be seen that the static pressure in the diffuser exit region is lower for the SA. The RSM-ω model shows a similar flow in the diffuser to that of the SST model, except the small separation at a bit further downstream than that of the SST model.

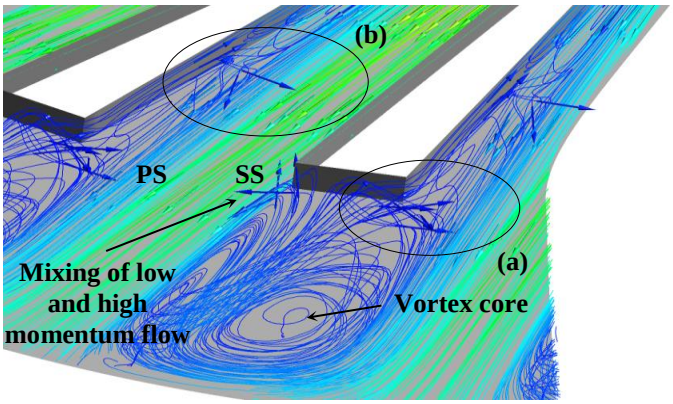

Fig. 6 Recirculating wake flow in the diffuser channel and downstream (SA model at P1)

Table 5 Wall clock time and number of iterations required at operating point P1

	SST	SST-CC	SA	RSM-SSG	RSM-ω
Wall clock (hrs)	5.27	12.00	11.90	11.00	18.76
Iterations	674	1155	1306	805	1382

6.4 COMPUTATIONAL TIME REQUIRED

Simulations were carried out using an Intel Xeon 8 core processor. The "platform MPI local parallel function" available within CFX was used to reduce computational time by utilising the total number of cores available.

The required wall clock time as well as the number of iterations to reach convergence are presented in Table 5. Clearly, the SST model is the most efficient with respect to time but also in terms of stability and robustness across the three operating points considered. Interestingly, the curvature correction has had a detrimental effect on the time required to reach convergence, contrary to Smirnov et al. [7] who noted that the convergence rate and total CPU time was

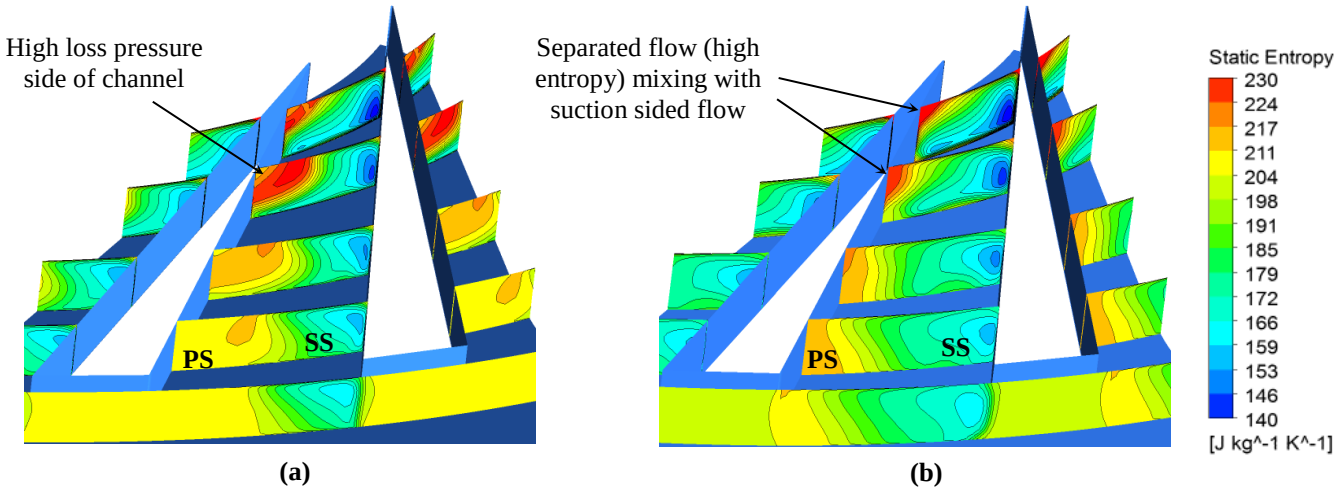

Fig. 7 Static entropy at several streamwise locations within the diffuser domain (a) SA, and (b) SST

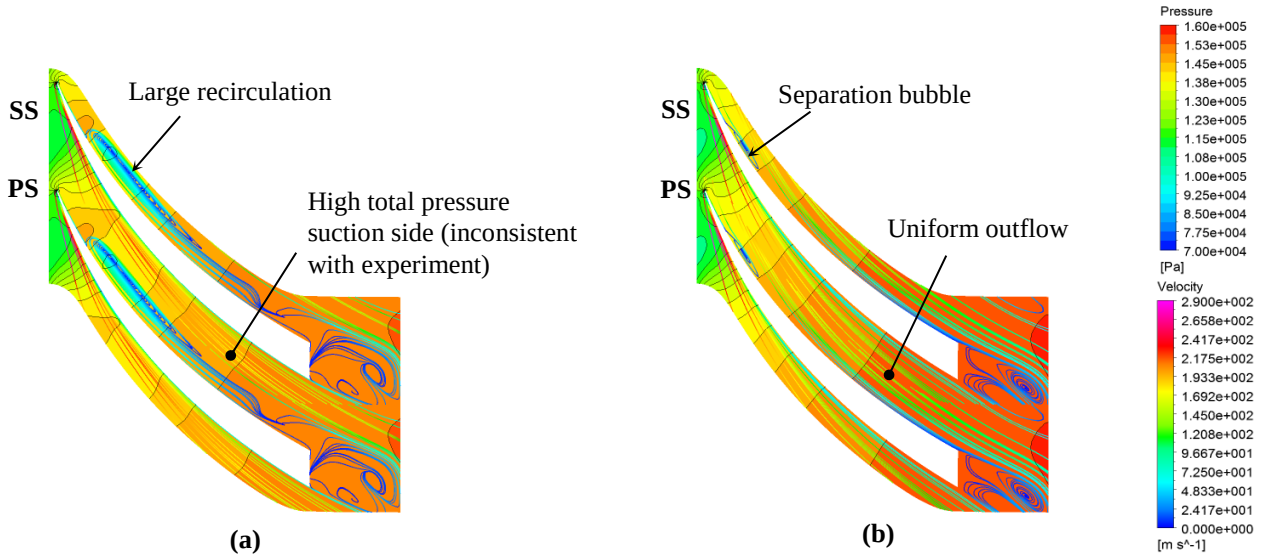

Fig. 8 Static pressure contour plot with streamlines at 95% span in the diffuser domain (a) SA, (b) SST

similar at all operating points between the two models. However, in this study a denser grid (1.35 times more elements) has been used and likely the difference between two is the solver struggling to resolve local instabilities. The most difficult model to reach convergence at each operating point was the RSM-ω in which the simulation had to be heavily relaxed to reach convergence. As expected, away from the surge condition, the SA is the most efficient with respect to wall clock time and number of iterations to convergence.

7 CONCLUSIONS AND RECCOMENDATIONS

A number of turbulence models (SA, SST, SST-CC, RSM-SSG and RSM-ω) have been assessed and compared to experimental data of the centrifugal compressor, Radiver. For the compressor overall performance parameters, each of the models assessed yielded good agreement with experimental results, where the discrepancy is well below 2% in most cases. The SST model provides accurate results over the entire speedline of the present test cases whilst keeping the solution time low. The increased accuracy in the prediction of pressure ratio and efficiency by the SST-CC model at lower mass flow rate compared to the original SST comes at the expense of a longer computing time (double in some cases). All Reynolds stress models were found to have a longer running time.

In terms of local flow field predictions, at the off-design operating condition, P1, the SST-CC provides the most accurate results for all four velocities considered at measurement plane 2M' (impeller exit, upstream of the interface), where comparable results are reported by the other eddy viscosity models. On the other hand, the Reynolds stress models typically over predict the velocity near the pressure side of the blade due to the high intensity tip leakage vortex predicted. The SA shows the least accuracy at this plane. At measurement plane 7M (at the diffuser exit, downstream of the interface), the RSM-ω predicts the flow structure of wake and separation for the operating point P1 in fair agreement with the experiment, where the total pressure is slightly more central and the pressure side wake is larger. On the other hand, the SA fails to predict the proper flow structures with high levels of separation beginning just

upstream of the diffuser throat. Consequently, this model predicts the static pressure and total-to-static efficiency least accurately. The SA predicts the work input by the impeller in excellent agreement with the experiment towards surge and the mid-point of the speedline and is also the least computationally expensive near the mid-point and choke condition. However, one-dimensional averaging of the variables to calculate performance parameters conceals the local flow features and does not imply good resolution thereof.

In conclusion, even though the SST-CC and RSM-ω showed better performance in complex flow prediction at off-design conditions, the SST model is reasonably stable, robust and time efficient to predict the basic local flow physics and provide good prediction of all performance parameters. The SA model is quick and provides comparable overall parameters. However, the SA shows some limits, such as the consistent under prediction of the static pressure at the outlet and inaccurate prediction of detailed flow structures. Therefore, the SA model is not recommended for detailed or advanced design stage prediction.

ACKNOWLEDGMENTS

The authors would like to thank the Institute of Jet Propulsion and Turbomachinery (IST) of RWTH Aachen, Germany, for providing the Radiver test case.

NOMENCLATURE

C_p	Specific heat capacity at constant pressure
$\dot{m}$	Mass flow rate
p	Static pressure
y^+	Dimensionless wall distance
U	Blade speed
γ	Ratio of specific heats
η	Efficiency
Π	Pressure ratio

SUBSCRIPTS

0	Stagnation/total property
1	Impeller inlet
2	Impeller outlet
2M	Upstream of diffuser leading edge
2M’	Within impeller passage
7M	Diffuser channel exit
8M	Outlet of computational model

ABRREVIATIONS

SST	Shear Stress Transport
RSM	Reynolds Stress Model
SA	Spalart-Allmaras
TR	Temperature ratio
PS	Pressure side
SS	Suction side

REFERENCES

[1] Wilcox, D.C. 2006, Turbulence Modelling for CFD, 3rd edn, DCW Industries, CA.

[2] ANSYS 2015, ANSYS CFX-Solver Theory Guide, 16.0th edn, ANSYS, Inc., Canonsburg, PA.

[3] Ziegler, K.U., Gallus, H.E. and Niehuis, R. 2003a, "A Study on Impeller-Diffuser Interaction—Part I: Influence on the Performance", ASME J. Turbomach., 125, pp. 173-182.

[4] Ziegler, K.U., Gallus, H.E. and Niehuis, R. 2003b, "A Study on Impeller-Diffuser Interaction—Part II: Detailed Flow Analysis", ASME J. Turbomach., 125, pp. 183-192.

[5] Bourgeois, J.A., Martinuzzi, R.J., Savory, E., Zhang, C. and Roberts, D.A. 2011, "Assessment of Turbulence Model Predictions for an Aero-Engine Centrifugal Compressor", J. Turbomach., 133, 011025.

[6] ANSYS 2015, ANSYS CFX Reference Guide, 16.0th edn, ANSYS, Inc., Canonsburg, PA.

[7] Smirnov, P.E., Thorsten, H. and Menter, F.R. 2007, "Numerical simulation of turbulent flows in centrifugal compressor stages with different radial gaps", ASME Turbo Expo 2007: Power for Land, Sea and Air, Montreal, Canada, pp.1029-1038.

[8] Sivagnanasundaram, S., Spence, S. and Early, J. 2013, "Map Width Enhancement Technique for a Turbocharger Compressor", J. Turbomach, 136, pp. 061002-061002.

[9] Menter, F.R., Kuntz, M. and Langstry, R. 2003, "Ten Years of Industrial Experience with the SST Turbulence Model", Turbulence, Heat and Mass Transfer 4, pp. 625-632.

[10] Smirnov, P.E. and Menter, F.R. 2009, "Sensitization of the SST Turbulence Model to Rotation and Curvature by Applying the Spalart–Shur Correction Term", J. Turbomach, 131, 041010.

[11] Spalart, P.R. and Shur, M.L. 1997, "On the Sensitization of Turbulence Models to Rotation and Curvature", Aerospace Science and Technology, 1, no. 5, pp. 297-302.

[12] Johnson, R.W. 1998, Handbook of Fluid Dynamics, 1st edn, CRC Press, Florida, USA.

[13] Fletcher, D.F., Geyer, P.E. and Haynes, B.S. 2009, "Assessment of the SST and Omega-Based Reynolds Stress Models for the Prediction of Flow and Heat Transfer in a Square-Section U-Bend", Computational Thermal Sciences: An International Journal, 1, no. 4, pp. 385-403.

[14] Ali, S., Elliott, K.J., Savory, E., Zhang, C., Martinuzzi, R.J. and Lin, W.E. 2015, "Investigation of the Performance of Turbulence Models With Respect to High Flow Curvature in Centrifugal Compressors", J. Fluids Engineering, 138, no. 5, 051101.